Journal of Biomedical Optics 7(3), 291–299 (July 2002)

Optical rotation and linear and circular depolarization rates in diffusively scattered light from chiral, racemic, and achiral turbid media

Kevin C. Hadley
University of Waterloo
Department of Chemistry
Waterloo, Ontario N2L 3G1, Canada

I. Alex Vitkin
Ontario Cancer Institute/University of Toronto
Departments of Medical Biophysics and Radiation Oncology
Toronto, Ontario M5G 2M9, Canada

Abstract. The polarization properties of light scattered in a lateral direction from turbid media were studied. Polarization modulation and synchronous detection were used to measure, and Mueller calculus to model and derive, the degrees of surviving linear and circular polarization and the optical rotation induced by turbid samples. Polystyrene microspheres were used as scatterers in water solutions containing dissolved chiral, racemic, and achiral molecules. The preservation of circular polarization was found to exceed the linear polarization preservation for all samples examined. The optical rotation induced increased with the chiral molecule concentration only, whereas both linear and circular polarizations increased with an increase in the concentrations of chiral, racemic, and achiral molecules. This latter effect was shown to stem solely from the refractive index matching mechanism induced by the solute molecules, independent of their chiral nature.
[DOI: 10.1117/1.1483880]

Keywords: polarization; multiple scattering; chirality; polarization modulation.

Paper JBO TP-14 received Mar. 8, 2002; revised manuscript received Mar. 14, 2002; accepted for publication Mar. 31, 2002.

1 Introduction

Many natural and synthetic systems have disordered properties that render them optically turbid. Examples abound in science, technology, medicine, and the natural environment, and include such diverse systems as interstellar gases, biological tissues, turbulent flows, colloidal suspensions, and microcrystalline solids. Optical examinations of these random media are challenging due to extensive multiple light scattering which scrambles potentially useful sample information encoded in the light beam. For example, most biological tissues are highly scattering at visible and near-infrared (IR) wavelengths,[1] so quantitative tissue spectroscopy and imaging are difficult. In recent investigations researchers have attempted to utilize the polarization properties of light to probe biological tissues and other random media, since diffusely scattered light is often partially polarized to an extent that can be experimentally detected. Several research groups are thus investigating the response of turbid media to polarized light by examining the polarization properties of multiply scattered light.[2–19] These polarization methodologies have been developed to study various aspects of polarized light interaction with turbid media, including the investigation of the depolarization mechanisms, quantification of depolarization length scales, determination of system Mueller matrices, and derivation of the Stokes parameters of scattered light. In several recent publications polarization imaging studies of multiply scattering media were described.[6,11,20–22]

Optical investigations of turbid media that contain chiral components have also been reported.[23–31] The interest in chiral turbid media is driven by the attractive possibility of noninvasive optical monitoring of the glucose level in diabetic patients. This is a very difficult unresolved problem in clinical medicine and an active area of research that utilizes different biomedical optics approaches.[32,33] For polarized light research, detection of glucose and quantification of its concentration rely on the molecule's chirality that stems from its asymmetric molecular structure, resulting in a number of characteristic effects generically called optical activity.[34] A well-known manifestation of optical activity is the ability of a glucose solution to rotate the plane of linearly polarized light about the axis of propagation. The amount of rotation depends on the molecular concentration, the pathlength through the medium, and the optical rotatory power at the interrogation wavelength.[35] This and other chiral asymmetries encoded in the polarization properties of light transmitted through largely transparent (nonscattering) media enable very sensitive and accurate determination of glucose concentrations. With turbid materials, however, the scattering effects dominate, loss of polarization information is significant, pathlengths get scrambled, and chiral effects stemming from a small amount of dissolved glucose are much more difficult to discern.

We have previously developed polarization modulation and synchronous detection methods to measure surviving polarization fractions in diffusive scattering even in the presence of large noisy depolarized backgrounds, such as in the case of synthetic turbid media[25,27,28,30,31] and *ex vivo*[28] and *in vivo*

Address all correspondence to I. Alex Vitkin.Tel: 416-946-4501, Ext. 5742; Fax: 416-946-6529; E-mail: alex.vitkin@rmp.uhn.on.ca

1083-3668/2002/$15.00 © 2002 SPIE

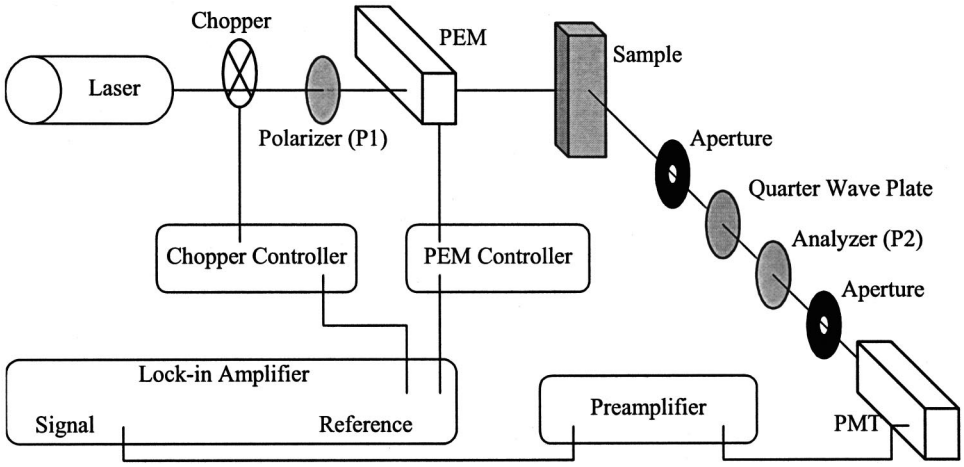

Fig. 1 Schematic of the apparatus for measuring degrees of polarization and optical rotation of scattered light. Arrangement B is shown. In arrangement A, the quarter wave plate is removed.

biological tissues.[31] Furthermore, we have experimentally observed chiral asymmetries due to the presence of glucose. Both varied the level of polarization preservation and the rotation of linearly polarized light fraction varied with glucose concentrations in the turbid samples.[25,27,28,30]

In comparing turbid microsphere suspensions with and without chiral molecules, depolarization was diminished in the former case both in the lateral and backscattering directions, although the mechanism responsible for this polarization enhancement effect was not determined. In this paper, we extend our methodology to perform this determination. Specifically, we analyze the polarization characteristics of laterally scattered light from chiral, racemic (equal amounts of oppositely handed isomers), and achiral solutions that contain scattering polystyrene microspheres in an effort to determine whether the chirality or the refractive index matching mechanism is the dominant cause of preservation of the enhanced polarization. We also develop methods to explicitly derive linear and circular degrees of polarization, and compare these depolarization rates in microsphere suspensions. Finally, the dependence of optical rotation of the linearly polarized light fraction on the chirality of the turbid medium is quantified.

2 Theory

Light of any arbitrary polarization state may be represented by a Stokes vector (**S**) of the form

$$\begin{bmatrix} I \\ Q \\ U \\ V \end{bmatrix}, \tag{1}$$

where I represents the total light intensity, Q and U represent the linearly polarized components of the beam, and V represents the circularly polarized component. The intensity I is directly measurable with a photodetector. For an arbitrary light beam, these terms are related by

$$I^2 \geq Q^2 + U^2 + V^2, \tag{2}$$

where the equality holds for fully polarized light, and the inequality applies to partially polarized light. The total degree of polarization (DOP) is defined as

$$\mathrm{DOP}_T = \sqrt{\frac{Q^2 + U^2 + V^2}{I^2}}. \tag{3}$$

The linearly polarized fraction is represented by the degree of linear polarization,

$$\mathrm{DOP}_L = \sqrt{\frac{Q^2 + U^2}{I^2}}. \tag{4}$$

The degree of circular polarization is similarly defined as

$$\mathrm{DOP}_T = \sqrt{\frac{V^2}{I^2}}. \tag{5}$$

Of interest in the current study were the linear and circular depolarizations that occurred due to multiple scattering within the turbid sample and the optical rotation of the linearly polarized light that may be induced by the chirality of the medium. The sample was thus illuminated with a polarized light beam whose incident polarization varied in a time-dependent, controlled fashion. Upon diffusive interactions with the scattering medium, the surviving polarization properties of the light were detected at 90°, synchronously with the incident polarization modulation. The surviving linear and circular polarization fractions, β_L and β_C, respectively, are defined in terms of the incident (subscript i) and scattered (subscript s) polarization states as

$$\beta_L = \frac{\mathrm{DOP}_{L,s}}{\mathrm{DOP}_{L,i}}, \tag{6}$$

$$\beta_C = \frac{\mathrm{DOP}_{C,s}}{\mathrm{DOP}_{C,i}}. \tag{7}$$

The layout of optical elements is schematically presented in Figure 1. There were two experimental arrangements employed for this study that differed in the analyzing elements

placed between the sample and the detector. In arrangement A, the analyzing optics consisted of a linear polarizer (analyzer) with pass axis $\theta°$ to the horizontal plane. Positive angles indicate rotation of the analyzer counterclockwise as one looks down the beam in the direction of its propagation. This arrangement was useful for determining the optical rotation α and the degree of linear polarization β_L. To extract the degree of circular polarization β_C, arrangement B was employed, which included a quarter wave plate with its fast axis 45° to the horizontal placed between the sample and the linear analyzer. The time-varying source of incident polarized light was furnished by passing linearly polarized laser light through a transparent quartz element of a photoelastic modulator (PEM). This device provides controlled, time-varying birefringence that converts the incoming linearly polarized light into transmitted elliptically polarized light,[36] the polarization states of which vary over time at the PEM's resonant frequency of 50 kHz. The use of this time-varying polarization modulation is useful in turbid media experiments because it enables high sensitivity measurements of weak polarization signals in a large noisy depolarized background using synchronous detection with a lock-in amplifier. After scattering interactions with the microsphere sample, photons directed 90° to the incident beam passed through analyzing elements and impinged on a polarization-insensitive detector.

To model the polarization effects in this experimental system, the various optical components were represented by Mueller matrices. Using Mueller calculus, an optical element that acts on a light beam is represented by multiplication of the incident light Stokes vector by the Mueller matrix for that optical element. The result is the Stokes vector of the transmitted beam. Mueller matrices for common optical elements, such as a linear polarizer, a quarter wave plate (QWP), and the PEM, are available in optics textbooks.[37,38] Representing the turbid chiral sample by a suitable matrix is more challenging, as described below.

The resultant Stokes vector for arrangement A is

$$(\mathbf{S})_{\mathrm{A}}=[\mathrm{P2}(\theta)]\ [\mathrm{sample}]\ (\mathrm{PEM})\ (\mathrm{P1})\ (\mathbf{S}_{\mathrm{i}});$$

similarly, for arrangement B,

$$(\mathbf{S})_{\mathrm{B}}=[\mathrm{P2}(\theta)]\ (\mathrm{QWP})\ (\mathrm{sample})\ (\mathrm{PEM})\ (\mathrm{P1})\ (\mathbf{S}_{\mathrm{i}}).$$

These expressions are now derived.

Following the passage of incident light through the 45° linear polarizer P1

$$\mathrm{P1}=\begin{bmatrix}1&0&1&0\\0&0&0&0\\1&0&1&0\\0&0&0&0\end{bmatrix},$$

and the PEM with its modulation axis horizontal is

$$\mathrm{PEM}=\begin{bmatrix}1&0&0&0\\0&1&0&0\\0&0&\cos\delta(t)&-\sin\delta(t)\\0&0&\sin\delta(t)&\cos\delta(t)\end{bmatrix},$$

the light incident on the sample has the following Stokes vector

$$\begin{bmatrix}1\\0\\\cos\delta(t)\\\sin\delta(t)\end{bmatrix},$$

$\delta(t)$ is the retardation of the PEM as a function of time, where $\delta=\delta_0\sin(2\pi ft)$. δ_0 is the maximum retardation imposed by the PEM, and f is the resonant frequency of its oscillation.

The turbid sample is modeled as an optical rotator (imposing a rotation of $\alpha°$) and a depolarizing element [imposing linear and circular depolarizations β_L and β_C, defined in Eqs. (6) and (7)]. The transmitted Stokes vector is thus

$$\begin{bmatrix}1\\\beta_L\sin(2\alpha)\cos\delta(t)\\\beta_L\cos(2\alpha)\cos\delta(t)\\\beta_C\sin\delta(t)\end{bmatrix}$$

$$=\begin{bmatrix}1&0&0&0\\0&\beta_L&0&0\\0&0&\beta_L&0\\0&0&0&\beta_C\end{bmatrix}\times\begin{bmatrix}1&0&0&0\\0&\cos(2\alpha)&\sin(2\alpha)&0\\0&-\sin(2\alpha)&\cos(2\alpha)&0\\0&0&0&1\end{bmatrix}\begin{bmatrix}1\\0\\\cos\delta(t)\\\sin\delta(t)\end{bmatrix}. \quad (8)$$

Two comments about the sample matrix are in order. First, although in general matrix multiplication is not commutative, in this case the order of multiplication of the two sample matrices does *not* matter. Second, the choice of sample matrix with different depolarization rates for linear (β_L) and circular (β_C) polarized light is an improvement over that in our previous work which modeled the sample with a generic depolarization parameter, β.[25,27,28,30,31] Although other depolarizer matrix formulations can be suggested, the current representation is relatively straightforward and is in line with reported observations of polarization-state dependent degrees of polarization in diffusive scattering.[6–8,16,19]

For arrangement A that employs a linear analyzer oriented $\theta°$ to the horizontal, information about the circular polarization state of the scattered light is lost, but the optical rotation α and the degree of linear polarization β_L can be determined with high precision. Multiplying the Stokes vector in Eq. (8) by the Mueller matrix for a linear polarizer oriented at $\theta°$, and selecting the resulting Stokes parameter I that represents the measured light intensity,

$$I_{\mathrm{A}}=k_{\mathrm{A}}\{1+\beta_L\sin[2(\alpha+\theta)]\cos\delta(t)\}, \quad (9)$$

where k_{A} is an unimportant experimental constant. The signal observed at the detector is thus a function of user-defined variables [the analyzer angle θ, the time varying PEM retardation $\delta(t)=\delta_0\sin(2\pi ft)$] and the sample unknowns (α and β_L) that can be obtained by fitting Eq. (9) to the experimental data.

For arrangement B, performing the additional multiplication with a Mueller matrix for a quarter wave plate with 45° fast axis orientation yields

$$I_B = k_B[1 + \beta_L \sin(2\theta)\cos(2\alpha)\cos\delta(t) + \beta_C \cos(2\theta)\sin\delta(t)]. \quad (10)$$

This expression contains all three important sample unknowns (α, β_L, and β_C), so the insertion of the quarter wave plate permits the determination of β_C as well. Note, however, that in contrast with Eq. (9), α and β_L now occur as a product of $\beta_L \cdot \cos(2\alpha)$, so independent determination of them appears difficult.

To facilitate the data analysis with the help of Eqs. (9) and (10), we expand the time-dependent retardation terms $\cos\delta(t)$ and $\sin\delta(t)$ in a series of spherical harmonics using the following expressions:[39]

$$\cos(z\sin\psi) = J_0(z) + 2\sum_{k=1}^{\infty} J_{2k}(z)\cos(2k\psi), \quad (11a)$$

$$\sin(z\sin\psi) = \sum_{k=0}^{\infty} J_{2k+1}(z)\sin[(2k+1)\psi], \quad (11b)$$

where J_n are the Bessel functions of the first kind of order n. Since lock-in amplification isolates signals at specific frequencies ($1f$ and $2f$ in these experiments), we expand the series up to the $2f$ terms, with $z = \delta_0$ and $\psi = 2\pi f$, to obtain

$$I_A = k_A\{1 + J_0(\delta_0)\beta_L \sin[2(\alpha+\theta)] + 2J_2(\delta_0) \times \beta_L \sin[2(\alpha+\theta)]\cos(2\pi\cdot 2f)\}, \quad (12)$$

$$I_B = k_B\{1 + J_0(\delta_0)\beta_L \sin(2\theta)\cos(2\alpha) + 2J_2(\delta_0) \times \beta_L \sin(2\theta)\cos(2\alpha)\cos(2\pi\cdot 2f) + 2J_1(\delta_0)\beta_C \cos(2\theta)\sin(2\pi\cdot 1f)\}. \quad (13)$$

In arrangement A, taking the ratio of the signal photocurrent component at $2f$ to the constant (dc) signal removes the experimental constant k_A and yields

$$(2f/\mathrm{dc})_A = \frac{2J_2(\delta_0)\beta_L \sin[2(\alpha+\theta)]}{1 + J_0(\delta_0)\beta_L \sin[2(\alpha+\theta)]}. \quad (14)$$

Thus, by dividing the signals at $2f$ by the signals at dc at a range of analyzer angles θ, parameters α and β_L can be extracted by fitting the data ratios to the curve described by Eq. (14).

Similarly, in arrangement B, the ratio of the signal at $1f$ to dc is

$$(1f/\mathrm{dc})_B = \frac{2J_1(\delta_0)\beta_C \cos(2\theta)}{1 + J_0(\delta_0)\beta_L \sin(2\theta)\cos(2\alpha)}. \quad (15)$$

And the $2f$/dc ratio is

$$(2f/\mathrm{dc})_B = \frac{2J_2(\delta_0)\beta_L \sin(2\theta)\cos(2\alpha)}{1 + J_0(\delta_0)\beta_L \sin(2\theta)\cos(2\alpha)}. \quad (16)$$

As mentioned above for arrangement B, the terms β_L and α appear together as the product of $\beta_L \cdot \cos(2\alpha)$ in Eqs. (15) and (16). This prevents independent determination of these two parameters. However, if α is small (less than a few degrees, a reasonable assumption for most biological applications), then $\cos(2\alpha) \sim 1$, and β_L can be determined. Making this assumption, β_C and β_L can be found using the $1f$/dc ratio described in Eq. (15). Then an additional determination of β_L can be performed by fitting Eq. (16) to the $2f$/dc signal ratios.

To summarize, the optical rotation α can only be measured in arrangement A. Also, this arrangement permits the measurement of β_L without the need to make any assumptions about the size of α. However, no information about circular polarization can be obtained from this setup. Insertion of a quarter wave plate in front of the linear analyzer (arrangement B) permits the determination of β_C and allows β_L to be evaluated with reasonable precision assuming a small induced optical rotation via a $1f$/dc data fit to Eq. (15). Also, with the same assumption about α, β_L can be independently estimated from a $2f$/dc fit to Eq. (16).

3 Experimental Methods

A schematic of the measurement system is shown in Figure 1. Unpolarized light from a HeNe laser ($\lambda = 632.8$ nm) passed through a linear polarizer oriented 45° to the vertical. The linearly polarized light traversed the PEM (Hinds, PEM-80), oriented with its modulation axis horizontal and modulation frequency f of 50 kHz. The resulting time-varying elliptically polarized light was incident on a 1-cm-sq quartz spectrophotometer cuvette that contained the liquid turbid suspension.

The detector arm was perpendicular to the incident beam, and consisted of a linear polarizer (analyzer) with its pass axis at θ° and a photomultiplier tube (PMT) (arrangement A). For arrangement B, a quarter wave plate with its fast axis at 45° was placed between the sample and the linear analyzer. Apertures (pinhole diaphragms) were located between the sample and the analyzing optical elements, and in front of the PMT, to limit the acceptance angle of the detector. The PMT signal was fed to a preamplifier (Stanford Research Systems, SR570) before entering the lock-in amplifier (Stanford Research Systems, SR350) which enabled detection of photocurrents at the PEM modulation frequency and its first harmonic ($1f$ and $2f$). The dc signal was measured by mechanically chopping the beam at low frequency of ~150 Hz and synchronously detecting it with the same preamp/lock-in amplifier pair.

Chiral samples consisted of $L-(+)$-arabinose (Sigma) dissolved in de-ionized water at concentrations up to ~2 M. Racemic samples were prepared from equal quantities of $L-(+)$-arabinose and $D-(+)$-arabinose by weight. Arabinose is a naturally occurring plant sugar similar to glucose. It was selected for these experiments because it has a significant specific rotatory power and because both its chiral isomers (L and D) are readily available and are inexpensive.

Achiral samples were prepared from glycerol (ACP) in distilled water at concentrations of up to ~35% glycerol by volume. These glycerol–water solutions were prepared to match the refractive index of the arabinose solutions. By comparing chiral and achiral samples of equal refractive index, the

influence of refractive index variations versus the influence of chirality of the molecules could be separated. The turbidity in all samples was provided by suspended polystyrene microspheres, 1.4 μm in diameter at a concentration of 0.2% (2 g/L).

By measuring signals at 2 f and dc in arrangement A at various angular settings of the analyzer, a plot of 2 f/dc vs θ was drawn for each sample. The θ range selected was 30°–150° to encompass a large part of the cyclic function of Eq. (14). The fitted value of α is particularly sensitive to data ratios in the rapidly changing region around 90°. A commercial software package was used for nonlinear curve fitting (SigmaPlot, Jandel Scientific Software) to extract α and β_L by fitting to Eq. (14). Peak PEM retardation δ_0 was set to 3.469 rad to generate relatively large values of $J_0(\delta_0)$ and $J_2(\delta_0)$. Maximizing these coefficients ensures a large amplitude of the 2 f/dc signal variation as a function of θ. This in turn makes the curve fit more sensitive to changes in β_L.

In arrangement B, analyzer angles from $-80°$ to $+80°$ were chosen to capture a large range of 1f/dc ratios. From these data, and assuming a small value of α, a two-parameter fit of β_C and β_L can be performed using Eq. (15). It should be noted that the small assumption for α only affects β_L, and the accuracy of the β_C determination remains unchanged.

It was also possible to make measurements at 2 f with this arrangement of the components. Using the same assumption of $\cos(2\alpha)\sim 1$, a single-parameter fit β_L was performed on a plot of 2 f/dc vs θ [Eq. (16)] as a check of the fit from the 1f/dc plot. δ_0 was set to 1.433 rad when collecting 1f/dc data and to 1.898 rad when collecting both 1f/dc and 2 f/dc data to generate relatively large values of $J_n(\delta_0)$ in Eqs. (15) and (16). Again, large Bessel function values lead to more sensitive fits of the parameters. As a check for the consistency of the three fitting techniques [Eqs. (14)–(16)], the values of β_L generated by each one can be compared.

4 Results and Discussion

Figure 2 shows results from a sample of 2 g/L suspension of 1.4 μm diam microspheres in pure de-ionized water. From a Mie scattering calculation,[40] this corresponds to a scattering coefficient μ_s of 73.1 cm^{-1}, scattering anisotropy g of 0.936, and reduced scattering coefficient μ_s' of 4.7 cm^{-1}. The vertical axis in Figure 2(a) is the ratio of the lock-in amplifier photocurrent at 2 f (100 kHz) to the dc signal measured at mechanical chopper frequency of 150 Hz. Negative ordinate values correspond to negative phase reading of the 2 f signal on the lock-in amplifier. The PEM retardation δ_0 was set to 3.469 rad to maximize the magnitude of the 2 f/dc ratio. The plotted points represents the experimental data ratios acquired with arrangement A; the line represents the theoretical best fit from Eq. (14). The fitting parameters were optical rotation α and the degree of linear polarization β_L, and the best fit was obtained with $\alpha=(1.43\pm 0.21)°$ and $\beta_L=(23.7\pm 0.2)\%$, with the nonlinear regression goodness-of-fit parameter $R^2=0.9992$. The quoted uncertainties represent standard deviations from the fitting routine. As seen from the close correspondence between experiment and theory, Eq. (14) describes the data well, and the values of α and β_L derived appear to be reasonable ($\alpha\sim 0°$, $\beta_L<100\%$, as would be expected for a turbid achiral sample). It is somewhat surprising that the optical rotation derived is not closer to zero; to investigate this further, we examined the specular reflection from a 45° metallic mirror placed on the sample platform (results not shown). This arrangement yielded $\alpha=(-0.08\pm 0.21)°$ and $\beta_L=(100.0\pm 0.2)\%$, with $R^2=0.9998$, very close to the theoretical values expected. This result validated the accuracy of the methodology, and ensured sound operation of the optical, electronic, and analytical fitting systems. The apparent offset in α of $\sim -1.4°$ from the microspheres-only turbid sample could be caused by some unknown sample birefringence or

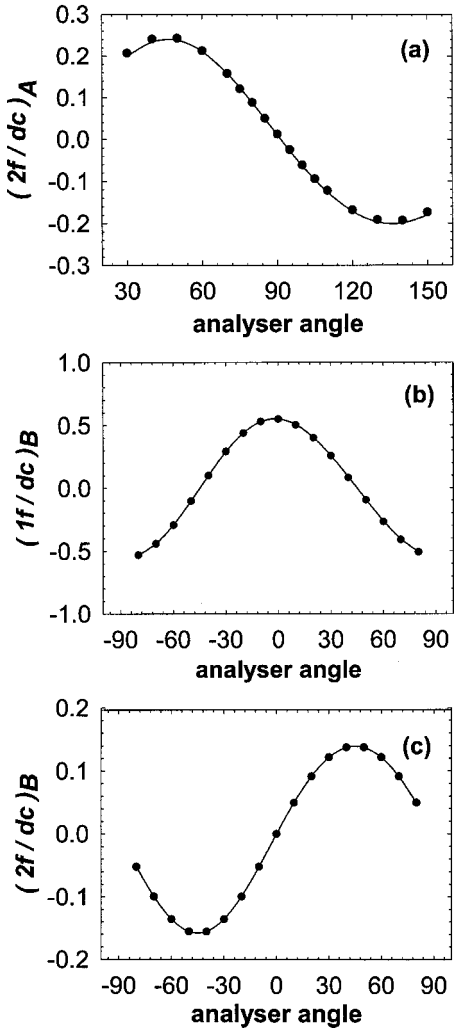

Fig. 2 (a) Variation in the 2f/dc values with the angular orientation of analyzer P2 for a turbid sample of 0.2% microspheres in de-ionized water. The points are the experimental data ratios in arrangement A (linear analyzer in the detector arm), and the line is the best fit using Eq. (14). The maximum PEM retardation amplitude was $\delta_0=3.469$ rad. The fitted values were $\alpha=-1.43\pm 0.21°$, $\beta_L=(23.7\pm 0.2)\%$, and $R^2=0.9992$. (b) 1f/dc ratios as a function of the P2 angle for the same sample, measured in arrangement B (quarter wave plate and linear polarizer in the detector arm). The fit is from Eq. (15), with $\beta_C=(47.4\pm 0.1)\%$, $\beta_L=(22.5\pm 0.6)\%$, and $R^2=0.9997$, assuming $\cos(2\alpha)\sim 1$. The PEM retardation setting was $\delta_0=1.898$ rad. (c) Corresponding 2f/dc measurements and fit via Eq. (16), using the same assumption of small α. This yields $\beta_L=(23.2\pm 0.1)\%$, and $R^2=0.9989$.

stray reflections from the cuvette walls. Although the true cause of this apparent optical rotation was not determined, its presence did not obscure interesting trends in α that resulted from increasing concentrations of chiral, achiral, and racemic molecules in the turbid suspensions.

To obtain the degree of circular polarization β_C, and to independently validate the derived value of β_L, the same turbid microsphere sample was examined in arrangement B. The PEM retardation δ_0 was set to 1.898 rad for this arrangement in order to maximize the magnitude of both the $1f/\mathrm{dc}$ and the $2f/\mathrm{dc}$ ratios. Figure 2(b) shows the $1f/\mathrm{dc}$ data ratios and the corresponding theoretical fit from Eq. (15). There are three unknowns in the fit, β_C, β_L, and α. As described in Sec. 2, the latter two always occur in combination $\beta_L \cdot \cos(2\alpha)$, so they cannot be determined independently from this analysis. Fortunately, setting $\cos(2\alpha)$ equal to unity resolves this ambiguity while introducing less than a ~3% error in β_L for even a reasonably large optical rotation of $\alpha \sim 4°$. When this is done, a two-parameter nonlinear regression fit to the data in Figure 2(b) yields $\beta_C = (47.4 \pm 0.1)\%$, $\beta_L = (22.5 \pm 0.2)\%$, and $R^2 = 0.9997$. The error in β_L is actually somewhat larger because of the assumption of $\cos(2\alpha) \sim 1$; nevertheless, the degree of linear polarization obtained is in good agreement with the value obtained above for arrangement A in Figure 2(a). Of note is the much larger degree of circular over linear polarization preservation for this turbid sample. This preferential retention of circular polarization has been reported previously in turbid samples with predominantly forward-peaked single scattering phase functions.[6–8,16,19,25] This is certainly the case for the current investigations, where Mie scattering calculations suggest that the 1.4-μm-diam polystyrene microspheres in water exhibit a scattering anisotropy parameter $g \sim 0.94$ at 632.8 nm, indicating predominantly forward scattering.[40] The preferential retention of circular over linear polarization states is further explored below within the context of chiral, achiral, and racemic turbid suspensions (Figure 5 below).

For completeness and a check of self-consistency, there is additional analysis that can be performed with arrangement B used in Figure 2(b). Figure 2(c) displays the $2f/\mathrm{dc}$ ratio obtained from the same experiment. The fit is performed using the expression in Eq. (16). Like above, the $\beta_L \cdot \cos(2\alpha)$ combination precludes independent determination of α and β_L. Again, assuming $\cos(2\alpha) \sim 1$, the one-parameter fit gives $\beta_L = (23.2 \pm 0.1)\%$, with $R^2 = 0.9989$. This result further corroborates the degrees of linear polarization derived in Figures 2(a) and 2(b).

We thus conclude that experimental arrangement B is better suited for an accurate determination of the degree of circular polarization β_C and a reasonably accurate determination of the degree of linear polarization β_L [by fitting the $1f/\mathrm{dc}$ data to Eq. (15); β_L can also be determined by fitting the $2f/\mathrm{dc}$ data to Eq. (16)]; if optical rotation is desired, the best approach is to remove the quarter wave plate and fit the resulting $2f/\mathrm{dc}$ data ratios to Eq. (14) like in arrangement A. Such a setup will also yield an accurate β_L value, which can serve as an additional check of the slightly less accurate values β_L derived with the λ/4 plate in place.

Having thus determined optimal ways in which to determine β_C, β_L, and α, we examine the dependence of these derived parameters on the properties of the turbid samples. Specifically, the preservation of enhanced polarization in turbid samples caused by the presence of dissolved chiral molecules has previously been reported.[25,27,28,30] Two putative explanations for this observed effect have been proposed. The electromagnetic (EM) wave propagation eigenmodes in a chiral medium are circular polarization states,[41] and circular polarization has been shown to be preferentially preserved in a medium with strong forward anisotropic scattering.[4,6] Alternatively, the solute-induced increase in the refractive index of the aqueous solution reduces the index mismatch of the suspended scatterers, making the samples less turbid[23,24] and thus lowering the depolarization rates. To determine which explanation is correct, we examine the degrees of polarization of light scattered from turbid suspensions containing (i) chiral molecules, (ii) racemic mixtures of chiral molecules, and (iii) achiral molecules, while matching the refractive indices of the aqueous phase of the three sample types. Figure 3 shows the degree of linear polarization β_L derived from measurements in arrangement A via Eq. (14). The three sets of symbols represent (i) 0–2 M *L*-arabinose chiral solution, (ii) a 50–50 *L*/*D* mixture of 0–2 M racemic arabinose solution, and (iii) 0%–35% (v/v) glycerol achiral solution. The horizontal axis represents the resultant common refractive index of the solutions. The trend of increasing β_L with an increase in the solution refractive index is clear, and it indicates that index matching lowers the turbidity of the medium and provides improved retention of linear polarization. For the range of refractive index values in Figure 3 over which the β_L is seen to double from ~23% to ~45%, the corresponding reduction in the scattering coefficients calculated from Mie theory is μ_s of 73.1 and 58.7 cm^{-1} (reduced scattering coefficient range μ_s' of 4.7 and 2.8 cm^{-1}). Note that, for a given refractive index, the chiral versus achiral nature of the solute does not affect the preservation of linear polarization. It thus appears that the chiral nature of the dissolved molecules is unimportant in enhancing the degree of linear polarization, and the

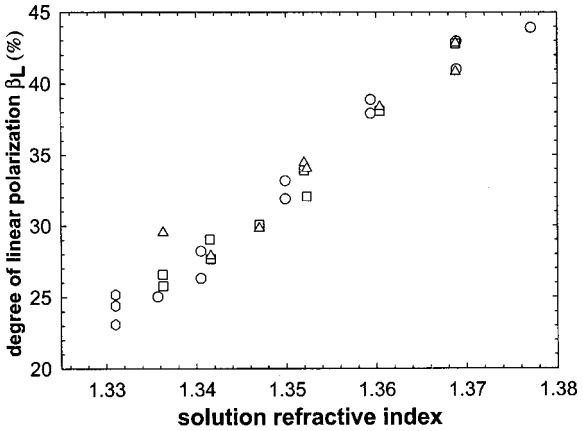

Fig. 3 Degree of linear polarization as a function of the refractive index of the aqueous phase of the turbid samples. β_L was determined from $2f/\mathrm{dc}$ measurements in arrangement A fitted with Eq. (14), as per Figure 2(a). The results are for chiral media (*L*-arabinose, squares), racemic media (*L*/*D* arabinose mixture, triangles), and achiral media (glycerol, circles). The microsphere suspension without any added solutes (at $n = 1.331$) is represented by hexagons. The error bars are smaller than the size of the symbols.

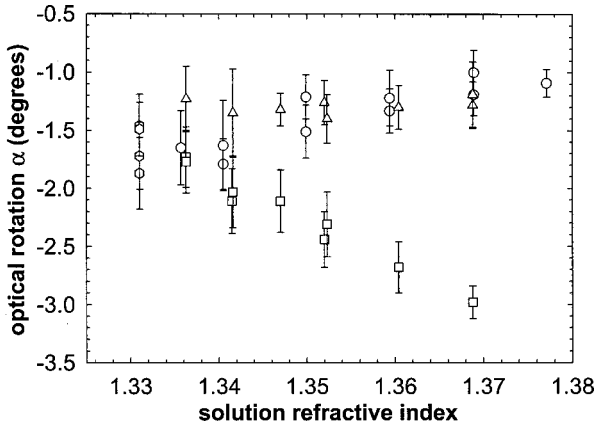

Fig. 4 Optical rotation α a function of the sample refractive index from the same data and fit as in Figure 3. The error bars represent regression-fit uncertainties in the optical rotations derived. The symbols are the same as those defined in Figure 3.

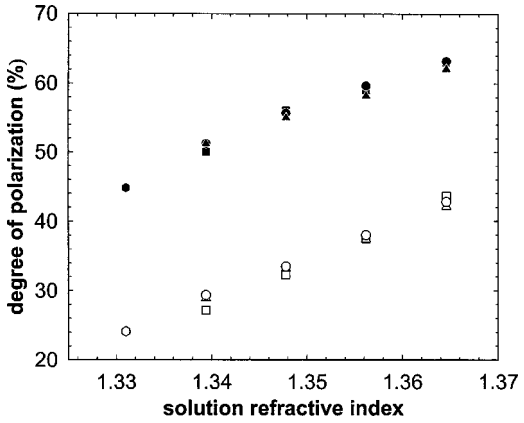

Fig. 5 Degree of circular polarization β_C (closed symbols) and degree of linear polarization β_L (open symbols) from chiral, racemic, and achiral turbid media. The results are from the $1f$/dc data ratios in arrangement B, fitted with Eq. (15) and assuming small α (see the text). The error bars are smaller than the size of the symbols. The symbol shapes have the same meaning as those in Figures 3 and 4.

effect is entirely due to refractive index matching.

Figure 4 summarizes the corresponding derived values of the optical rotation α as a function of the solution's refractive index. These results are from the same data set and fit as those in Figure 3. There is a small offset of the optical rotations (approximately $-1.5°$) that we have not been able to explain nor eliminate. As well, the uncertainty in α is considerably greater than that in β as is evident by the size of the error bars in Figure 3. This indicates a much more sensitive dependence of functions in Eqs. (14)–(16) on β than on α. Nonetheless, of interest are the trends in optical rotation noted for each solute type. For both the racemic arabinose mixtures and the achiral glycerol solutions of equal refractive index, the optical rotation induced by the sample remained essentially constant, independent of the solute concentration. This was expected, since racemic mixtures and achiral solutes should not induce optical rotation. The apparent slight upward trend is probably related to the unexplained α offset noted above. For chiral solutions of $L-(+)$-arabinose, the optical rotation observed increased in a linear fashion with the concentration of solute. These results imply that the methodology developed is capable of measuring small optical rotations of linearly polarized light even in diffusive scattering. While the preservation of linear polarization is insensitive to the chiral nature of the molecules, measurements of optical rotation may reveal if the dissolved solute is chiral or achiral/racemic.

Figure 5 shows the dependence of circular polarization β_C and linear polarization β_L as a function of the solution refractive index. These results are from experimental measurement with the quarter wave plate in place (arrangement B), analyzed with Eq. (15) at the $1f$/dc signal, as per Figure 2(b). Both degrees of polarization are seen to increase by $\sim$23% in a strikingly linear fashion. Like in Figure 3, the surviving polarization fractions seems to be solely a function of the solution refractive index. Chirality of the solute had no visible effect on β_L or β_C. Again, this suggests that the increase in β_L or β_C is the result of a smaller difference between the refractive index of the solution and that of the suspended polystyrene microspheres. This smaller refractive index difference decreases the turbidity of the medium, resulting in less depolarization.

The difference in levels of polarization preservation for linearly versus circularly polarized light is significant; the latter appears greater by approximately a factor of 2 across the entire refractive index range (corresponding to a scattering coefficient range of μ_s of $73.1-61.3\ \mathrm{cm}^{-1}$, and a reduced scattering coefficient range μ_s' of $4.7-3.1\ \mathrm{cm}^{-1}$). This preferential retention of circular over linear polarization states has been noted before in media composed of predominantly forward-scattering particles.[4,6,7,16,19,25] In the current turbid samples, the anisotropy parameter $g\sim0.94$, so scattering is certainly forward peaked, and the larger magnitude of β_C compared to β_L is not surprising. However, one must exercise caution in extrapolating these microsphere scattering results to biological tissues. The differences in the nature of refractive index variation in the two systems, including the potential contribution of dependent scattering, can lead to a variety of unexpected effects, including larger magnitudes of β_L compared to β_C.[16,19] Even within the microsphere system, the relative magnitude of the two depolarization parameters is predicted to depend sensitively on the size (and thus the scattering anisotropy) of the inclusions.[7,8] Further studies are planned to measure β_L and β_C parameters in a variety of turbid systems, including those of biological origin.

5 Summary and Conclusions

A methodology for determining the optical rotation, the degree of linear polarization, and the degree of circular polarization of light diffusely scattered from turbid media was developed, and was applied to determine the cause of the previously reported chirality-induced increase in the preservation of polarization. The chiral nature of the dissolved solutes was only evident in the derived optical rotations, which were seen to increase linearly with chiral molecule concentrations but stayed essentially constant with increasing concentrations of achiral or racemic additives. The observed increase in the linear and circular degrees of polarization with dissolved sol-

utes in turbid suspensions was caused by the refractive-index matching effect and was shown to be independent of the molecular chirality. Circularly polarized light was preserved to a greater extent ($\sim 2\times$) than linearly polarized light in all turbid samples examined.

The capability to measure polarization properties of multiply scattered light is exciting in that it yields several experimental observables which can be used to study and characterize turbid systems. Parameters such as optical rotation and the degrees of (linear, circular) polarization can be determined with high sensitivity even in the presence of a large depolarized background, for example, using polarization modulation and synchronous detection techniques. The potential sensitivity of these parameters to weak chiral asymmetries is important for conceptual and for practical reasons, such as noninvasive detection of chiral glucose molecules in turbid biological tissues. Much work remains to be done in the effort to determine the applicability of the methodology developed to this difficult clinical problem. The physiological concentrations of blood glucose is ~ 1 g/L, hence the optical rotation for a typical physiological measurement would be $\sim 10^{-3}$ deg; this is $\sim 40\times$ smaller than the current α detection limit estimated from Figures 2 and 4. However, chiral molecules also affect the derived degrees of linear and circular polarizations, so there may be ways of inferring glucose concentrations from β results as well.[27] In future research we will address the optimal selection of experimental observables best suited for sensitive detection of small concentrations of chiral inclusions, the incorporation of tissue linear birefringence and spatial inhomogeneity into polarization models, and evaluation of the confounding effects of other optically active species present in biological media.

Acknowledgments

The financial support of the Natural Sciences and Engineering Research Council of Canada (NSERC) and Photonics Research Ontario (PRO) is gratefully acknowledged.

References

1. W.-F. Cheung, S. A. Prahl, and A. J. Welch, ''A review of optical properties of biological tissues,'' *IEEE J. Quantum Electron.* **26**, 2166–2185 (1990).
2. M. P. van Albada and A. Lagendijk, ''Observation of weak localization of light in a random medium,'' *Phys. Rev. Lett.* **55**, 2692–2695 (1985).
3. P. E. Wolf and G. Maret, ''Weak localization and coherent backscattering of photons in disordered media,'' *Phys. Rev. Lett.* **55**, 2696–2699 (1985).
4. F. C. MacKintosh, J. X. Zhu, D. J. Pine, and D. A. Weitz, ''Polarization memory of multiply scattered light,'' *Phys. Rev. B* **40**, 9342–9345 (1989).
5. R. Berkovits and M. Kaveh, ''The vector memory effects for waves,'' *Europhys. Lett.* **13**, 97–101 (1990).
6. J. M. Schmitt, A. H. Gangjbakhche, and R. F. Bonner, ''Use of polarized light to discriminate short-path photons in multiply scattering medium,'' *Appl. Opt.* **31**, 6535–6546 (1992).
7. S. Martinez and R. Maynard, ''Polarization statistics in multiple scattering of light: A Monte Carlo approach,'' in *Photonic Band Gaps and Localization*, C. M. Souloukis, Ed., pp. 99–114, Plenum, New York (1993).
8. D. Bicout, C. Brosseau, A. S. Martinez, and J. M. Schmitt, ''Depolarization of multiply scattered waves by spherical diffusers: Influence of size parameter,'' *Phys. Rev. E* **49**, 1767–1770 (1994).
9. M. Dogariu and T. Asakura, ''Photon pathlength distribution from polarized backscattering in random media,'' *Opt. Eng.* **35**, 2234–2239 (1996).
10. A. H. Hielscher, J. R. Mourant, and I. J. Bigio, ''Influence of the particle size and concentration on the diffuse backscattering of polarized light from tissue samples and biological cell suspensions,'' *Appl. Opt.* **36**, 125–135 (1997).
11. S. G. Demos and R. R. Alfano, ''Optical polarization imaging,'' *Appl. Opt.* **36**, 150–155 (1997).
12. H. Hilescher, A. A. Eick, J. R. Mourant, D. Shen, J. P. Freyer, and I. J. Bigio, ''Diffuse backscattering Mueller matrices of highly scattering media,'' *Opt. Express* **1**, 441–454 (1997).
13. A. Ambirajan and D. C. Look, ''A backward Monte Carlo study of the multiple scattering of a polarized light beam,'' *J. Quant. Spectrosc. Radiat. Transf.* **58**, 171–192 (1997).
14. D. Cameron, M. J. Rakovic, M. Mehrubeouglu, G. Kattawar, S. Rastegar, L. V. Wang, and G. L. Cote, ''Measurement and calculation of the two-dimensional backscattering Mueller matrix of a turbid medium,'' *Opt. Lett.* **23**, 485–487 (1998).
15. M. J. Rakovic and G. W. Kattawar, ''Theoretical analysis of polarization patterns from incoherent backscattering of light,'' *Appl. Opt.* **37**, 3333–3338 (1998).
16. V. Sankaran, M. J. Everett, D. J. Maitland, and J. T. Walsh, ''Comparison of polarized light propagation in biological tissues and phantoms,'' *Opt. Lett.* **24**, 1044–1046 (1999).
17. G. Yao and L. H. Wong, ''Two-dimensional depth-resolved Mueller matrix characterization of biological tissue by optical coherence tomography,'' *Opt. Lett.* **24**, 537–539 (1999).
18. S. Bartel and A. H. Hielscher, ''Monte Carlo simulations of the diffuse backscattering Mueller matrix for highly scattering media,'' *Appl. Opt.* **39**, 1580–1588 (2000).
19. V. Sankaran, J. T. Walsh, and D. J. Maitland, ''Polarized light propagation through tissue phantoms containing closely packed scatterers,'' *Opt. Lett.* **25**, 239–241 (2000).
20. S. L. Jacques, M. Ostermeyer, L. H. Wang, and D. V. Stephens, ''Polarized light transmission through skin using video reflectometry: Toward optical tomography of superficial tissue layers,'' *Proc. SPIE* **2671**, 199–210 (1996).
21. M. P. Silverman and W. Strange, ''Object delineation within turbid media by backscattering of phase-modulated light,'' *Opt. Commun.* **144**, 7–11 (1997).
22. S. L. Jacques, J. R. Roman, and K. Lee, ''Imaging superficial tissues with polarized light,'' *Lasers Surg. Med.* **26**, 199–129 (2000).
23. J. S. Meyer, S. A. Walker, S. Fantini, M. A. Franceschini, and E. Gratton, ''Possible correlation between blood glucose concentration and the reduced scattering coefficient of tissues in the near infrared,'' *Opt. Lett.* **19**, 2062–2064 (1994).
24. M. Kohl, M. Cope, M. Essenpreis, and D. Bocker, ''Influence of glucose concentration on light scattering in tissue-simulating phantoms,'' *Opt. Lett.* **19**, 2170–2173 (1994).
25. M. P. Silverman, W. Strange, J. Badoz, and I. A. Vitkin, ''Enhanced optical rotation and diminished depolarization in diffusive scattering from a chiral liquid,'' *Opt. Commun.* **132**, 410–416 (1996).
26. F. Madarasz, D. Engelhaupt, J. Wyly, and J. Milelli, ''Photonic molecular probe,'' U.S. Patent, No. 5,871,442 (filed 1997, granted 1999).
27. I. A. Vitkin and E. Hoskinson, ''Polarization studies in multiply scattering chiral media,'' *Opt. Eng.* **39**, 353–362 (2000).
28. R. C. N. Studinski and I. A. Vitkin, ''Methodology for examining polarized light interactions with tissues and tissuelike media in the exact backscattering direction,'' *J. Biomed. Opt.* **5**, 330–337 (2000).
29. X. Wang, G. Yao, and L. H. Wang, ''Monte Carlo model and single-scattering approximation of the propagation of polarized light in turbid media containing glucose,'' *Appl. Opt.* **41**, 792–801 (2001).
30. I. A. Vitkin, R. D. Laszlo, and C. L. Whyman, ''Effect of molecular asymmetry of optically active molecules on the polarization properties of multiply scattered light,'' *Opt. Express* **10**, 222–229 (2002).
31. A. Vitkin and R. C. N. Studinski, ''Polarization preservation in diffusive scattering from *in vivo* turbid biological media: Effects of tissue optical absorption in the exact backscattering direction,'' *Opt. Commun.* **190**, 37–43 (2001).
32. J. McNickols and G. L. Cote, ''Optical glucose sensing in biological fluids: an overview,'' *J. Biomed. Opt.* **5**, 5–16 (2000).
33. A. J. Berger, ''Optical sensing of glucose,'' *Opt. Photonics News* **22**, S23–S28 (2001).
34. L. D. Barron, *Molecular Light Scattering and Optical Activity*, Cambridge University Press, London (1982).

35. J. Applequist, ''Optical activity: Biot's bequest,'' *Am. Sci.* **75**, 59–67 (1987).
36. J. C. Kemp, ''Piezo-optical birefringence modulators: New use for a long-known effect,'' *J. Exp. Theor. Phys.* **59**, 950–954 (1969).
37. E. Collett, *Polarized Light: Fundamentals and Applications*, Dekker, New York (1993).
38. C. Brosseau, *Fundamentals of Polarized Light: A Statistical Optics Approach*, Wiley, New York (1998).
39. M. Abramowitz and I. A. Stegun, *Handbook of Mathematical Functions*, p. 361, Dover, New York (1965).
40. C. F. Bohren and D. R. Huffman, *Absorption and Scattering of Light by Small Particles*, Appendix A, Wiley Interscience, New York (1983).
41. A. Lakhtakia, *Beltrami Fields in Chiral Media*, World Scientific, Singapore (1994).